coatings

MDPI

Article

In Situ Synthesis of High Thermoelectric Performance Bi_2Te_3 Flexible Thin Films through Thermal Diffusion Engineering

Ning Chen [1], Dongwei Ao [2,3,*], Junji Guo [4], Wenke Bao [2,*], Yuexing Chen [1] and Zhuanghao Zheng [1]

[1] Shenzhen Key Laboratory of Advanced Thin Films and Applications, Key Laboratory of Optoelectronic Devices and Systems of Ministry of Education and Guangdong Province, College of Physics and Optoelectronic Engineering, Shenzhen University, Shenzhen 518060, China; 2200451012@email.szu.edu.cn (N.C.); chenyx@szu.edu.cn (Y.C.); zhengzh@szu.edu.cn (Z.Z.)
[2] School of Machinery and Automation, Weifang University, Weifang 261061, China
[3] School of Chemical Engineering and Technology, Tianjin University, Tianjin 300072, China
[4] School of Mathematics and Physics, Henan University of Urban Construction, Pingdingshan 467036, China; guojunji@buaa.edu.cn
* Correspondence: aodongwei@wfu.edu.cn (D.A.); bwk2016@yeah.net (W.B.)

Abstract: Bi_2Te_3-based materials are promising candidates for near-room-temperature applications due to their high thermoelectric performance and low cost. Here, an innovative thermal diffusion strategy combined with magnetron sputtering and thermal evaporation methods was employed to fabricate Bi_2Te_3 flexible thin films (f-TFs) on a flexible polyimide substrate. An in situ synthesis of Bi_2Te_3 f-TFs with good crystallinity was obtained using a straightforward thermal diffusion method through diffusion of Te into a Bi precursor under low vacuum conditions (1×10^5 Pa). This method offers easy preparation, low cost, and a large-area film preparation for industrialization. The electrical conductivity increases with increasing thermal diffusion temperatures. A high room temperature carrier mobility of ~28.7 cm^{-2} V^{-1} S^{-1} and an electrical conductivity of ~995.6 S cm^{-1} can be achieved. Then, a moderate room temperature Seebeck coefficient >100 μV K^{-1} was obtained due to the chemical stoichiometry being close to the standard by optimizing the thermal diffusion temperature. Consequently, a maximum room temperature PF of ~11.6 μW cm^{-1} K^{-1} was observed in Bi_2Te_3 f-TFs prepared using a thermal diffusion temperature of 653 K. The thermal diffusion strategy applied in the thin film preparation represents an effective approach for the preparation of high thermoelectric performance Bi_2Te_3 f-TFs, offering a promising route for future thermoelectric applications.

Keywords: thermoelectric; Bi_2Te_3; flexible thin film; thermal diffusion

check for updates

Citation: Chen, N.; Ao, D.; Guo, J.; Bao, W.; Chen, Y.; Zheng, Z. In Situ Synthesis of High Thermoelectric Performance Bi_2Te_3 Flexible Thin Films through Thermal Diffusion Engineering. *Coatings* **2023**, *13*, 2018. https://doi.org/10.3390/coatings13122018

Academic Editor: Ihor S. Virt

Received: 9 November 2023
Revised: 27 November 2023
Accepted: 27 November 2023
Published: 29 November 2023

Copyright: © 2023 by the authors. Licensee MDPI, Basel, Switzerland. This article is an open access article distributed under the terms and conditions of the Creative Commons Attribution (CC BY) license (https://creativecommons.org/licenses/by/4.0/).

1. Introduction

Thermoelectric technology can convert thermal and electrical energy, which is expected to be used in portable and wearable electronic devices [1–5]. The efficiency of thermoelectric materials is quantitatively evaluated by the dimensionless figure of merit (ZT) = $S^2\sigma T/\kappa$ [6], where S, σ, κ, and T represent the Seebeck coefficient, the electrical conductivity, the thermal conductivity, and the absolute temperature, respectively [7,8]. Owing to the challenges inherent in measuring the κ of thin films, the power factor (PF) = $S^2\sigma$ has been used to evaluate the electric performance [9]. Materials such as SnSe (12.8 μW cm^{-1} K^{-1}, ≈350 K) [10], Cu2Se (≈17 μW cm^{-1} K^{-1}, 400 K) [11], AgSbTe2 (≈19 μW cm^{-1} K^{-1}, 550 K) [11,12], Ag2Se (19.36 μW cm^{-1} K^{-1}, 300 K) [13], PbS (20.58 μW cm^{-1} K^{-1}, 473 K) [14], Sb2Te3 (21 μW cm^{-1} K^{-1}, 300 K) [15], GeTe (40.8 μW cm^{-1} K^{-1}, 623 K) [16], and STN (54 μW cm^{-1} K^{-1}, ≈750 K) [17] are well known for their excellent thermoelectric properties. Bi_2Te_3 materials remain ideal candidates for room-temperature applications due to their excellent room-temperature properties and low cost [18–26].

In recent research, various material engineering strategies, such as defect engineering [27,28], energy band engineering [29], nanoengineering [30,31], and texturing engineering [32], have significantly enhanced the thermoelectric efficiency of thin films. For instance, Feng et al. [27] improved the thermoelectric properties of Bi_2Te_3 thin films by incorporating excess Te through defect engineering, and the PF improved significantly, from approximately 1.8 to 4.65 μW cm^{-1} K^{-2}. Lan et al. [28] applied a pulsed electric field to C-doped Bi_2Te_3 films, improving their defect structures and thus increasing the PF from approximately ~15 to 22.5 μW cm^{-1} K^{-2}. Chen et al. [29] effectively reduced the energy band gap through Se doping of Bi_2Te_3 and improved the S to −160 μV/K. Additionally, the PF increased to 15 μW cm^{-1} K^{-2}. Yabuki et al. [30] synthesized integrated nanocomposite films by embedding single-walled carbon nanotubes into Bi_2Te_3 nanoflakes, and the PF notably increased to 1.38 μW cm^{-1} K^{-2}.

A range of thin film deposition techniques, including screen printing [32], solvothermal methods [33], and magnetron sputtering [34,35], have been utilized to fabricate high-performance n-type Bi_2Te_3-based flexible thin films (f-TFs). Notably, Varghese et al. [32] synthesized Bi_2Te_3 nanocrystal inks via a microwave-assisted wet chemical approach for screen printing onto polyimide substrates. Subsequent cold pressing and sintering led to thermoelectric films that achieved a PF of approximately 5.65 at 448 K. Rani et al. [33] produced Bi_2Te_3 nanostructures through solvothermal methods, attaining a PF of 6.5 μW cm^{-1} K^{-2} at 385 K. He et al. [34] fabricated Bi_2Te_3 f-TFs through direct current magnetron sputtering with in situ annealing, achieving a PF of 8.2 μW cm^{-1} K^{-2}. Furthermore, Joo et al. [35] generated Bi_2Te_3 f-TFs using radiofrequency co-sputtering at 573 K and recorded a PF of 9.7 μW cm^{-1} K^{-2}. In our previously published work [36], we successfully synthesized high-quality Te-embedded Bi_2Te_3 f-TFs by using magnetron sputtering in combination with the thermal diffusion method. To further optimize the chemical content of Bi_2Te_3 f-TFs and improve its thermoelectric performance, the process can be further optimized to prepare Te through thermal evaporation, with the aim of achieving full sublimation of the Te and Bi-Te reaction.

In this study, a thermal diffusion process combined with thermal evaporation and magnetron sputtering was employed to prepare n-type Bi_2Te_3 f-TFs on polyimide (PI) substrates, as shown in Figure 1a. The thermal diffusion method can provide sufficient energy for the growth of Bi_2Te_3 crystals, significantly improving carrier transport performance [36]. The Bi film was deposited using magnetron sputtering, and the Te film was deposited using thermal evaporation methods. Evaporating Te film results in a higher preparation efficiency, which is more uniform and makes it easier to produce large-area thin films than magnetron sputtering. Additionally, the copper mold is more conducive to Te sublimation and the Bi-Te reaction. Figure 1b shows a schematic diagram of the Te diffusion into Bi to react to form Bi_2Te_3 during thermal diffusion. Thermal diffusion is the mutual diffusion reaction between Bi and Te to form Bi_2Te_3. Te sublimation and diffusion speed are faster due to the high saturated vapor pressure of Te. Bi_2Te_3 film is on the Bi precursor film after thermal diffusion, while there is no residue of materials in the Te precursor film due to the complete sublimation of Te induced by a high saturated vapor pressure. The σ increased with increasing thermal diffusion temperatures (T_{diff}) due to the improved carrier mobility induced by the weak carrier scattering. The maximum σ of ~995.6 S cm^{-1} was achieved at T_{diff} = 653 K. By optimizing the T_{diff}, a S > 95 μV K^{-1} can be obtained due to the reasonable chemical content regulation. Consequently, a room-temperature *PF* of ~11.6 μW cm^{-1} K^{-2} can be achieved in Bi_2Te_3 f-TFs under T_{diff} = 653 K. The *PF* value of our prepared Bi_2Te_3 f-TFs is competitive with those of films prepared by other scholars, as shown in Figure 1c. And the *PF* value of the prepared thin film is only slightly lower than the previously reported *PF* value of 14.65 μW cm $^{-1}$ K^{-2} [36]. The novelty thermal diffusion method has the advantages of easy preparation, low cost, and large-area film preparation. In this work, the ultra-high performance of the as-prepared intrinsic Bi_2Te_3 thin film was not achieved due to the lack of regulation. It is expected to achieve significant performance improvement through doping or structural regulation in the future.

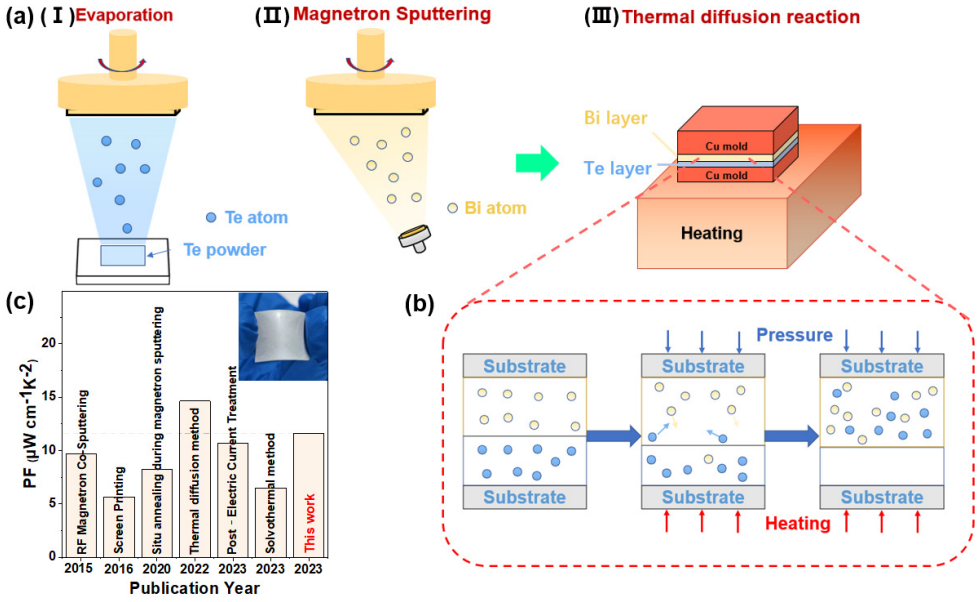


Figure 1. (**a**) Schematic diagram of Bi_2Te_3 f-TFs preparation process. Section (**I**) outlines the thermal evaporation process of Te. Section (**II**) details the magnetron sputtering process of Bi. Section (**III**) describes the thermal diffusion process. (**b**) Schematic diagram of detailed illustration of the thermal diffusion reaction. (**c**) Evolution of the power factor (PF) in Bi_2Te_3-based thin films, as demonstrated by various fabrication methods: RF magnetron co-sputtering (2015) [35], screen printing (2016) [32], in situ annealing during magnetron sputtering (2020) [34], thermal diffusion method (2022) [36], post-electric current treatment (2023) [37], solvothermal method (2023) [33]. Inset is the image of the Bi_2Te_3 f-TFs.

2. Methods and Experimental Design

2.1. Thin Film Preparation

A thermal diffusion method combined with thermal evaporation methods was employed to synthesize n-type Bi_2Te_3 thin films on a flexible PI substrate. High purity tellurium power (99.99%, Macklin, Shanghai, China) weighing 0.6 g was used to deposit the Te film on the PI substrate using thermal evaporation methods, as shown in section I of Figure 1a. The thermal evaporation parameters were as follows: a thermal evaporation power of 20 W, an evaporation time of 13 min, and a thermal evaporation pressure of 5×10^{-5} Torr. The thickness of the as-deposited Te film was ~500 nm. A high purity Bismuth target (99.99%) was used to deposit the Bi precursor film on the PI substrate using magnetron sputtering methods, as shown in section II of Figure 1a. The magnetron sputtering parameters were as follows: a radio frequency power of 25 W, a duration of 30 min, and a working pressure of 1 Pa. The thickness of the Bi film was ~150 nm. Subsequently, both the Te and Bi films were pressurized in a copper mold placed on the heating equipment in a glove box (1×10^5 Pa), as shown in section III of Figure 1a. Compared to the high vacuum experimental conditions used in our previous work [36], this experimental method is conducive to large-scale production. The T_{diff} was set to 608 K, 623 K, 638 K, and 653 K, respectively. The as-deposited n-type Bi_2Te_3 f-TFs is shown in the inset of Figure 1c.

2.2. Characterization of the Thin Film

The crystalline structure of the sample was investigated using X-ray diffraction (XRD, D/max 2500, Rigaku Corporation, Tokyo, Japan, utilizing CuKα radiation). Scanning electron microscopy (SEM, Zeiss-spra 55, Oberkochen, Baden-Württemberg, Germany) and SEM coupled with energy dispersive spectroscopy (SEM-EDS, Bruker Quantax 200, Billerica, MA, USA) were used to analyze the surface morphology and chemical composition. The Hall properties were measured using a Hall measurement system (HL5500PC, Nanometrics,

Ottawa, ON, Canada), while the S and σ values were measured using a SBA458 system (Nezsch, Selb, Bavaria, Germany).

3. Results and Discussion

To elucidate the crystalline structure of the Bi_2Te_3 f-TFs prepared through thermal diffusion, an XRD analysis was employed, and XRD spectra are shown in Figure 2a. All the XRD peaks can be indexed to Bi_2Te_3 (PDF #15-0863). It can be seen that the three main diffraction peaks correspond to the (006), (015), and (0010) planes of Bi_2Te_3. The strongest (015) peaks suggest a preferred orientation, as shown in Figure 2a and Section I of Figure 2a. As well, the intensity of the (015) diffraction peaks increased with increasing T_{diff}, indicating the increase in crystallinity. Te peaks (PDF #36-1452) can be observed in Figure 2a. The enlarged (012) and (110) Te peaks in Section II of Figure 2a further confirm the existence of Te. The obvious Te peak appears in the Bi_2Te_3 f-TFs prepared at $T_{diff} > 623$ K. More Te atoms can be sublimated and diffused into the Bi precursor thin film at a high T_{diff}. The over-sublimated Te remained in the Bi precursor during cooling, leading to the formation of Te.

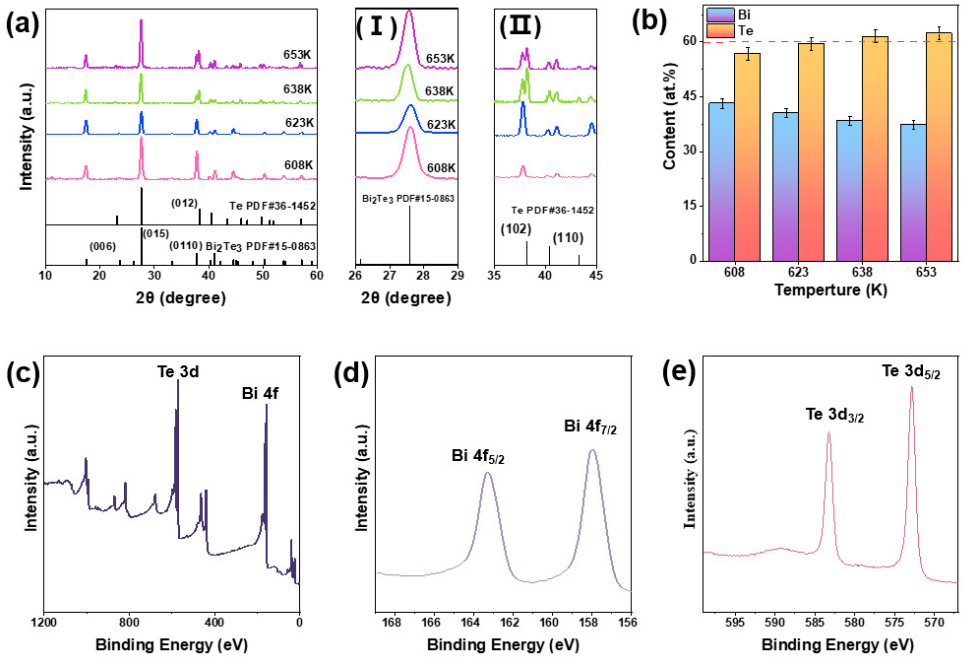


Figure 2. (**a**) XRD spectra of the as-prepared Bi_2Te_3 f-TFs. Inset (**I**) highlights the enlarged (015) peaks of Bi_2Te_3; inset (**II**) presents the enlarged (012) and (110) peaks of Te. (**b**) The measured chemical contents of Bi and Te. (**c**) The XPS full spectra. (**d**,**e**) The XPS spectra of Bi and Te, respectively.

To further understand the Te content evolution, a detailed semi-quantitative investigation of Te can be measured in Figure 2b. As can be seen, the Te content increases and Bi content decreases with increasing T_{diff}. At T_{diff} = 608 K, the low Te content of Bi_2Te_3 is attributed to the poor diffusion reaction. When the T_{diff} increased to 623 K, the chemical content of Bi and Te was close to the standard chemical content of Bi_2Te_3 (40% and 60%) due to the fully thermal diffusion process. When T_{diff} increased to over 638 K, the Te content was above 60% due to the Te over-sublimation. This Te-rich content is consistent with the XRD results. To further characterize the valence states of Sb and Te in the Bi_2Te_3 f-TFs, XPS studies were employed, as shown in Figure 2c–e. The typical binding energy of Bi and Te can be observed in the XPS full spectra, as shown in Figure 2c. The binding energies at 157.0 eV and 162.3 eV correspond to Bi $4f_{7/2}$ and Bi $4f_{5/2}$, respectively, as shown in Figure 2d, indicating a Bi valence state of +3. The binding energies at 572.9 eV and 583.3 eV correspond to $Te3d_{5/2}$ and $Te3d_{7/2}$, respectively, as shown in Figure 2d, suggesting a Te valence state of −2. The XPS spectra further prove the formation of Bi_2Te_3.

The surface and cross-section morphology of the Bi_2Te_3 f-TFs was analyzed using SEM technology, as shown in Figure 3. The uniformly distributed nanoparticles of the Bi_2Te_3 f-TFs prepared at T_{diff} = 608 K, 623 K, 638 K, and 653 K can be observed in Figure 3a–d, respectively. This well-crystallized structure is consistent with the XRD results. The size of the Bi_2Te_3 particles increased with increasing T_{diff}. Finally, the large flake-like particles could be obtained at T_{diff} > 638 K, as shown in Figure 3d, indicating a high crystallinity. The cross-section SEM images of Bi_2Te_3 f-TFs are shown in Figure 3e. Highly dense crystals could be observed in all the Bi_2Te_3 f-TFs. And the thicknesses of the Bi_2Te_3 f-TFs prepared at T_{diff} = 608 K, 623 K, 638 K, and 653 K were ~293 nm, ~386 nm, ~300 nm, and ~280 nm, respectively. Figure 3f exhibits the SEM-BSE of the Bi_2Te_3 f-TFs prepared at T_{diff} = 653 K and the corresponding EDS mapping. As can be seen, most of the Bi and Te elements were uniformly distributed. Minor Te-enriched regions can be observed, as shown the marked white circle, resulting from over-sublimation of Te in Bi_2Te_3. The EDS maps further validated the Te-embedded Bi_2Te_3 composite film.

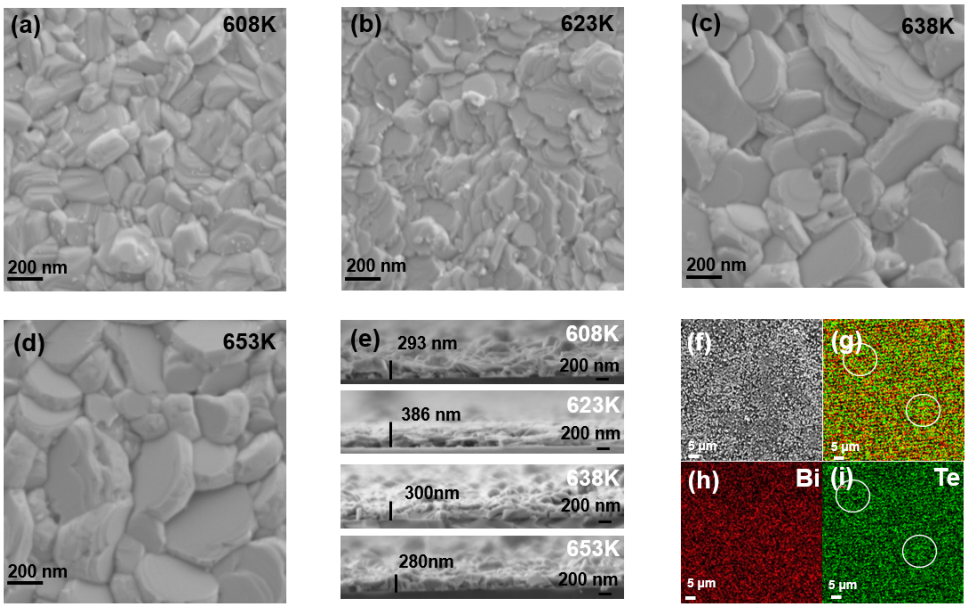


Figure 3. (**a**–**d**) SEM images of Bi_2Te_3 f-TFs prepared at T_{diff} = 608 K, 623 K, 638 K, and 653 K, respectively. (**e**) The corresponding cross-sectional SEM images of Bi_2Te_3 f-TFs. (**f**–**i**) The SEM-BSE of Bi_2Te_3 f-TFs prepared at T_{diff} = 653 K and the corresponding EDS maps. BSE: Backscattered electron.

Figure 4 shows the electrical performances of the as-prepared Bi_2Te_3 f-TFs synthesized at different T_{diff}. The temperature-dependent σ of Bi_2Te_3 f-TFs is shown in Figure 4a. As can be seen, σ decreased with increasing T, and the maximum σ was achieved at room temperature. When T_{diff} increased from 608 K to 653 K, the room-temperature σ significantly increased from ~359.19 S cm^{-1} to ~995.6 S cm^{-1}. To further understand the electric performance evolution, the Hall performance of Bi_2Te_3 f-TFs was investigated. The single parabolic band (SPB) model was employed to analyze the electrical performance. The n_e-dependent μ curves calculated using the SPB model are shown in Figure 4b. The μ increased with increasing T_{diff}, leading to an increase in σ. Correspondingly, the deformation potential coefficient (E_{def}) decreased with increasing T_{diff}, as shown in Figure 4c. This is consistent with the increase in μ, potentially resulting from reduced carrier scattering in the Te-embedded Bi_2Te_3 heterostructure. Compared to the highest σ of 567.69 S cm^{-1} in our previous work [36], the high σ in this work is due to the decreased energy filtration effect caused by the composition approaching the standard stoichiometric ratio. Figure 4d plots the T-dependent S, and the negative S values confirm the traditional n-type semiconductor behavior. Additionally, S exhibited a decreasing trend with increasing T_{diff} values from 608 K to 653 K. All the room-temperature S values were above 100 μV K^{-1} due to the

near standard stoichiometric ratio, and the maximum S of −151.95 μV K^{-1} in Bi_2Te_3 f-TFs prepared at T_{diff} = 608 K was obtained. n_e decreased with increasing T from 608 K to 638 K, and then n_e slightly increased. It can be seen that the change in S is attributed to the changes in n_e, regardless of the effective mass (m^*) evolution. Figure 4f shows the T-dependent PF, and the largest PF values were obtained at room temperature. The PF value of Bi_2Te_3 f-TFs prepared at T_{diff} = 653 K was obviously higher than that of T_{diff} < 638 K. The largest PF of ~11.6 μW cm^{-1} K^{-2} was achieved at T_{diff} = 653 K due to the corresponding high σ and S. As T_{diff} further increased, the thermoelectric performance decreased due to severe chemical content segregation, as shown in the Figure S1 and Table S1.

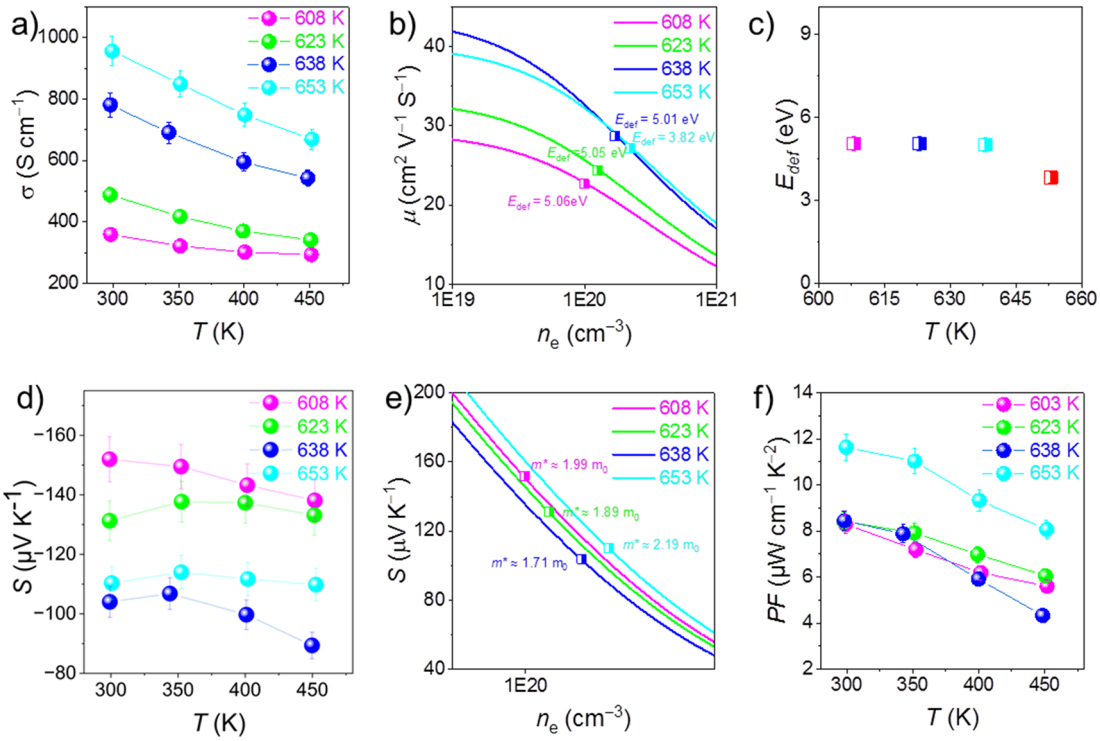


Figure 4. The thermoelectric performance of Bi_2Te_3 f-TFs: (**a**) T-dependent σ. (**b**) n_e-dependent μ. (**c**) T-dependent E_{def}. (**d**) T-dependent S. (**e**) n_e-dependent S. (**f**) T-dependent PF.

4. Conclusions

In this research, we successfully synthesized Bi_2Te_3 f-TFs with good crystallinity using a specialized thermal diffusion strategy combined with magnetron sputtering and thermal evaporation methods. The σ increased with increasing T due to the increase in μ induced by the decrease in E_{def}. The maximum room-temperature σ of ~995.6 S cm^{-1} was obtained at T_{diff} = 653 K. By optimizing T_{diff}, a near-standard stoichiometric ratio can be achieved, leading to a moderate S > 100 μV K^{-1}. Finally, a high room-temperature PF reached ~11.6 μW cm^{-1} K^{-2} due to the high σ and S. The successful preparation of thin films at low vacuum levels is particularly beneficial for large-scale production of thin films.

Supplementary Materials: The following supporting information can be downloaded at: https://www.mdpi.com/article/10.3390/coatings13122018/s1, Figure S1: The thermoelectric performance of Bi_2Te_3 prepared at 668 K; Table S1: The atomic percent of Bi_2Te_3 prepared at 668 K.

Author Contributions: N.C. and D.A made substantial contributions to the conceptualization, design of methodology, and writing—original draft. D.A. and Z.Z. provided administration. J.G., Y.C. and W.B. performed data acquisition, provided administrative, technical, and supervision, support, and reviewed and edited the manuscript. All authors have read and agreed to the published version of the manuscript.

Funding: This work was supported by the National Natural Science Foundation of China (No. 62274112), Guangdong Basic and Applied Basic Research Foundation (2022A1515010929), Natural Science Foundations of Shandong Province (ZR2023ME001), China Postdoctoral Science Foundation (2023M732609), and the Science and Technology plan project of Shenzhen (JCYJ20220531103601003).

Institutional Review Board Statement: Not applicable.

Informed Consent Statement: Not applicable.

Data Availability Statement: Data are contained within the article and supplementary materials.

Conflicts of Interest: The authors declare no conflict of interest.

References

1. Guo, Y.; Li, Y.; Zhang, Q.; Wang, H. Self-powered multifunctional UV and IR photodetector as an artificial electronic eye. *J. Mater. Chem. C* **2017**, *5*, 1436–1442. [CrossRef]
2. Jia, Y.; Jiang, Q.; Sun, H.; Liu, P.; Hu, D.; Pei, Y.; Liu, W.; Crispin, X.; Fabiano, S.; Ma, Y.; et al. Wearable Thermoelectric Materials and Devices for Self-Powered Electronic Systems. *Adv. Mater.* **2021**, *33*, 2102990. [CrossRef] [PubMed]
3. Xu, C.; Song, Y.; Han, M.; Zhang, H. Portable and wearable self-powered systems based on emerging energy harvesting technology. *Microsyst. Nanoeng.* **2021**, *7*, 25. [CrossRef] [PubMed]
4. Burmistrov, I.; Khanna, R.; Gorshkov, N.; Kiselev, N.; Artyukhov, D.; Boychenko, E.; Yudin, A.; Konyukhov, Y.; Kravchenko, M.; Gorokhovsky, A.; et al. Advances in Thermo-Electrochemical (TEC) Cell Performances for Harvesting Low-Grade Heat Energy: A Review. *Sustainability* **2022**, *14*, 9483. [CrossRef]
5. Sun, W.; Liu, W.-D.; Li, L.; Wang, D.-Z.; Yin, L.-C.; Li, M.; Shi, X.-L.; Liu, Q.; Chen, Z.-G. Performance optimization of a dual-thermoelectric-liquid hybrid system for central processing unit cooling. *Energy Convers. Manag.* **2023**, *290*, 117222. [CrossRef]
6. Shi, X.; Chen, L.D. Thermoelectric materials step up. *Nat. Mater.* **2016**, *15*, 691–692. [CrossRef] [PubMed]
7. Dresselhaus, M.S.; Chen, G.; Tang, M.Y.; Yang, R.G.; Lee, H.; Wang, D.Z.; Ren, Z.F.; Fleurial, J.P.; Gogna, P. New Directions for Low-Dimensional Thermoelectric Materials. *Adv. Mater.* **2007**, *19*, 1043–1053. [CrossRef]
8. Sun, W.; Liu, W.-D.; Liu, Q.; Chen, Z.-G. Advances in thermoelectric devices for localized cooling. *Chem. Eng. J.* **2022**, *450*, 138389. [CrossRef]
9. Shi, X.-L.; Zou, J.; Chen, Z.-G. Advanced Thermoelectric Design: From Materials and Structures to Devices. *Chem. Rev.* **2020**, *120*, 7399–7515. [CrossRef]
10. Su, L.Z.; Wang, D.Y.; Wang, S.N.; Qin, B.C.; Wang, Y.P.; Qin, Y.X.; Jin, Y.; Chang, C.; Zhao, L.D. High thermoelectric performance realized through manipulating layered phonon-electron decoupling. *Science* **2022**, *375*, 1385–1389. [CrossRef]
11. Liu, W.-D.; Yang, L.; Chen, Z.-G. Cu_2Se thermoelectrics: Property, methodology, and device. *Nano Today* **2020**, *35*, 100938. [CrossRef]
12. Roychowdhury, S.; Ghosh, T.; Arora, R.; Samanta, M.; Xie, L.; Singh, N.K.; Soni, A.; He, J.Q.; Waghmare, U.V.; Biswas, K. Enhanced atomic ordering leads to high thermoelectric performance in AgSbTe. *Science* **2021**, *371*, 722–727. [CrossRef]
13. Hu, Q.-X.; Liu, W.-D.; Zhang, L.; Sun, W.; Gao, H.; Shi, X.-L.; Yang, Y.-L.; Liu, Q.; Chen, Z.-G. SWCNTs/Ag2Se film with superior bending resistance and enhanced thermoelectric performance via in situ compositing. *Chem. Eng. J.* **2023**, *457*, 141024. [CrossRef]
14. Liu, Z.; Hong, T.; Xu, L.; Wang, S.; Gao, X.; Chang, C.; Ding, X.; Xiao, Y.; Zhao, L.D. Lattice expansion enables interstitial doping to achieve a high average ZT in n-type PbS. *Interdiscip. Mater.* **2022**, *2*, 161–170. [CrossRef]
15. Wei, M.; Shi, X.L.; Zheng, Z.H.; Li, F.; Liu, W.D.; Xiang, L.P.; Xie, Y.S.; Chen, Y.X.; Duan, J.Y.; Ma, H.L.; et al. Directional Thermal Diffusion Realizing Inorganic Sb2Te3/Te Hybrid Thin Films with High Thermoelectric Performance and Flexibility. *Adv. Funct. Mater.* **2022**, *32*, 2207903. [CrossRef]
16. Yin, L.C.; Liu, W.D.; Li, M.; Wang, D.Z.; Wu, H.; Wang, Y.; Zhang, L.; Shi, X.L.; Liu, Q.; Chen, Z.G. Interstitial Cu: An Effective Strategy for High Carrier Mobility and High Thermoelectric Performance in GeTe. *Adv. Funct. Mater.* **2023**, *33*, 2301750. [CrossRef]
17. Acharya, M.; Jana, S.S.; Ranjan, M.; Maiti, T. High performance (ZT>1) n-type oxide thermoelectric composites from earth abundant materials. *Nano Energy* **2021**, *84*, 105905. [CrossRef]
18. Zhu, B.; Liu, X.; Wang, Q.; Qiu, Y.; Shu, Z.; Guo, Z.; Tong, Y.; Cui, J.; Gu, M.; He, J. Realizing record high performance in n-type Bi_2Te_3-based thermoelectric materials. *Energy Environ. Sci.* **2020**, *13*, 2106–2114. [CrossRef]
19. Ahmad, K.; Almutairi, Z. Enhanced thermoelectric properties of bismuth telluride (Bi_2Te_3) and multiwall carbon nanotube (MWCNT) composites. *Mater. Today Commun.* **2023**, *35*, 106228. [CrossRef]
20. Wang, Z.; Cui, W.; Yuan, H.; Kang, X.; Zheng, Z.; Qiu, W.; Hu, Q.; Tang, J.; Cui, X. Direct ink writing of Bi_2Te_3-based thermoelectric materials induced by rheological design. *Mater. Today Energy* **2023**, *31*, 101206. [CrossRef]
21. Tang, X.; Li, Z.; Liu, W.; Zhang, Q.; Uher, C. A comprehensive review on Bi_2Te_3-based thin films: Thermoelectrics and beyond. *Interdiscip. Mater.* **2022**, *1*, 88–115. [CrossRef]
22. Shi, Q.; Li, J.; Zhao, X.; Chen, Y.; Zhang, F.; Zhong, Y.; Ang, R. Comprehensive Insight into p-Type Bi_2Te_3-Based Thermoelectrics near Room Temperature. *ACS Appl. Mater. Interfaces* **2022**, *14*, 49425–49445. [CrossRef] [PubMed]
23. Tan, M.; Liu, W.-D.; Shi, X.-L.; Sun, Q.; Chen, Z.-G. Minimization of the electrical contact resistance in thin-film thermoelectric device. *Appl. Phys. Rev.* **2023**, *10*, 021404. [CrossRef]

24. Lan, M.; Sun, S.; Liu, S.; Li, G.; Wang, Z.; Wang, Q. Controlling the shape of hexagonal structure by growth condition improves the thermoelectric properties of p-type Bi-Te films. *J. Eur. Ceram. Soc.* **2023**, *43*, 7493–7498. [CrossRef]
25. Moshtaghi, F.; Yousefpour, M.; Habibolahzadeh, A. Electrodeposition and characterization of poly-aniline-Bi-Te-Se-Sb thin films with thermoelectric properties. *Mater. Sci. Eng. B* **2023**, *296*, 116712. [CrossRef]
26. Rawther, A.N.; Rout, U.; Kumar, P.; Ramanathan, R.; Mallik, R.C. Thermoelectric properties of sputter deposited Bi_2Te_3–PbTe multilayer thin films. *Phys. B Condens. Matter* **2024**, *673*, 415467. [CrossRef]
27. Feng, J.; Zhu, W.; Zhang, Z.; Cao, L.; Yu, Y.; Deng, Y. Enhanced Electrical Transport Properties via Defect Control for Screen-Printed Bi_2Te_3 Films over a Wide Temperature Range. *ACS Appl. Mater. Interfaces* **2020**, *12*, 16630–16638. [CrossRef]
28. Lan, M.; Sun, S.; Liu, S.; Li, G.; Guo, H.; Wang, Q. Improved thermoelectric properties of C-doped Bi_2Te_3 films following short-range atomic diffusion induced by pulsed electric field treatment. *Ceram. Int.* **2022**, *48*, 26865–26873. [CrossRef]
29. Chen, Y.-X.; Zhang, J.-Z.; Nisar, M.; Abbas, A.; Li, F.; Liang, G.-X.; Fan, P.; Zheng, Z.-H. Realizing high thermoelectric performance in n-type Bi_2Te_3 based thin films via post-selenization diffusion. *J. Mater.* **2023**, *9*, 618–625. [CrossRef]
30. Yabuki, H.; Yonezawa, S.; Eguchi, R.; Takashiri, M. Flexible thermoelectric films formed using integrated nanocomposites with single-wall carbon nanotubes and Bi_2Te_3 nanoplates via solvothermal synthesis. *Sci. Rep.* **2020**, *10*, 17031. [CrossRef] [PubMed]
31. Liu, W.-D.; Yin, L.-C.; Li, L.; Yang, Q.; Wang, D.-Z.; Li, M.; Shi, X.-L.; Liu, Q.; Bai, Y.; Gentle, I.; et al. Grain boundary re-crystallization and sub-nano regions leading to high plateau figure of merit for Bi_2Te_3 nanoflakes. *Energy Environ. Sci.* **2023**, *16*, 5123–5135. [CrossRef]
32. Varghese, T.; Hollar, C.; Richardson, J.; Kempf, N.; Han, C.; Gamarachchi, P.; Estrada, D.; Mehta, R.J.; Zhang, Y. High-performance and flexible thermoelectric films by screen printing solution-processed nanoplate crystals. *Sci. Rep.* **2016**, *6*, 33135. [CrossRef] [PubMed]
33. Rani, K.; Gupta, V.; Ranjeet; Pandey, A. Improved thermoelectric performance of Se-doped n-type nanostructured Bi_2Te_3. *J. Mater. Sci. Mater. Electron.* **2023**, *34*, 1074. [CrossRef]
34. He, Z.; Chen, Y.-X.; Zheng, Z.; Li, F.; Liang, G.; Luo, J.; Fan, P. Enhancement of thermoelectric performance of N-type Bi_2Te_3 based thin films via in situ annealing during magnetron sputtering. *Ceram. Int.* **2020**, *46*, 13365–13371. [CrossRef]
35. Joo, S.-J.; Kim, B.S.; Min, B.-K.; Oh, M.W.; Lee, J.-E.; Ryu, B.K.; Lee, H.W.; Park, S.D. Deposition of n-Type Bi_2Te_3 Thin Films on Polyimide by Using RF Magnetron Co-Sputtering Method. *J. Nanosci. Nanotechnol.* **2015**, *15*, 8299–8304. [CrossRef]
36. Ao, D.W.; Liu, W.D.; Chen, Y.X.; Wei, M.; Jabar, B.; Li, F.; Shi, X.L.; Zheng, Z.H.; Liang, G.X.; Zhang, X.H.; et al. Novel Thermal Diffusion Temperature Engineering Leading to High Thermoelectric Performance in Bi_2Te_3-Based Flexible Thin-Films. *Adv. Sci.* **2021**, *9*, 2103547. [CrossRef]
37. Ao, D.; Liu, W.-D.; Ma, F.; Bao, W.; Chen, Y. Post-Electric Current Treatment Approaching High-Performance Flexible n-Type Bi_2Te_3 Thin Films. *Micromachines* **2022**, *13*, 1544. [CrossRef]

Disclaimer/Publisher's Note: The statements, opinions and data contained in all publications are solely those of the individual author(s) and contributor(s) and not of MDPI and/or the editor(s). MDPI and/or the editor(s) disclaim responsibility for any injury to people or property resulting from any ideas, methods, instructions or products referred to in the content.